15

Kirkpatrick-Baez focusing system for synchrotron applications

© D.G. Reunov,[1] A.D. Akhsakhalyan,[1] E.I. Glushkov,[1] I.P. Dolbnya,[2] I.G. Zabrodin,[1] I.A. Kaskov,[1] I.V. Malyshev,[1] M.S. Mikhailenko,[1] E.V. Petrakov,[1] A.E. Pestov,[1] V.N. Polkovnikov,[1] A.K. Chernyshev,[1] N.I. Chkhalo[1]

[1]Institute for physics of microstructure RAS,
603087 Afonino village, Kstov district, Nizhny Novgorod region, Russia
[2]Diamond Light Source, United Kingdom,
OX11 0DE, Oxfordshire, Didcot, Harwell Science and Innovation Campus
e-mail: reunov_dima@ipmras.ru

Received May 29, 2025
Revised May 29, 2025
Accepted May 29, 2025

The paper describes the Kirkpatrick–Baez focusing system for the 4+ generation synchrotron source based on the Siberian Ring Photon Source. The system is designed to operate in the photon energy range of 10–30 keV and should provide a submicron-sized focusing spot. The design principles and composition of the focusing system, as well as the technique for measuring the focusing spot size are reported. A brief description of the key problems and methods used in creating this system is given. The results of testing the focusing properties of the system obtained using a laboratory setup and the first experimental set of elliptical mirrors are presented. The minimum focusing spot size was about 5.2 μm, which, taking into account the size of the laboratory source and the quality of the collimating optics of the setup, will correspond to a focusing spot of about 2.6 μm on the synchrotron. The reasons for the discrepancy between the calculated and experimental data are discussed.

Keywords: synchrotron, ring photon source, focusing, Kirkpatrick–Baez system.

DOI: 10.61011/TP.2025.10.62086.124-25n

Introduction

In recent years, there have been rapid growth and construction of new generation synchrotron radiation (SR) sources. The 4+ generation Siberian Circular Photon Source (SCPS) will be launched in the nearest future. The 1–1 „Mikrofokus“, station will be implemented in one of its channels to solve fundamental and application tasks using a high-intensity X-ray beam with submicron focusing [1]. To solve the X-ray focusing problem, the Kirkpatrick–Baez (KB) glazing incidence X-ray optics was chosen. The KB focusing system [2–7] is an effective solution for precision SR control that is used in experiments requiring high spatial resolution in hard X-ray range. The system is based on a combination of two perpendicular (crossed system) elliptical mirrors to achieve high-accuracy focusing of X rays providing low aberrations. KB focusing system mirrors have a form of an elliptical cylinder with platinum coating for operation in a wide spectral range.

Several engineering and technological problems should be solved at the focusing system design and fabrication stage to make mirrors with effective roughness of 2 Å and RMS shape deviation ~ 1 nm to give an angular error $\leq 1\,\mu$rad, which are necessary to achieve submicron focusing of hard X-ray radiation.

Metrology of large-size mirrors is the first serious problem. Mirror length was 200 mm due to the glazing incidence configuration and the need for covering a significant part of the SR beam. In most cases, the size of the mirrors to be fabricated exceeds the aperture of an interferometer used to measure a surface shape.

The second problem is in complexity of interpreting interferometric measurements of surface shape. Surface curvature is so large that interference is observed only in a small part of surface. Both problems are solved by using a technology where small frames from different regions are crosslinked on a substrate followed by whole surface map recovery.

The third problem is the fabrication of such mirrors with a nanometer or even subnanometer mirror shape deviation from the desired design profile. This problem is resolved using an ion-beam shaping method. This method implements surface material removal through an aperture mask that cuts out the necessary beam region to form a uniform removal profile along the short side of a mirror. Mirror profile along the long side is formed by uneven reciprocating movement of the workpiece. The final stage involves correction of local shape errors.

And the second problem is in final alignment and qualification of the KB system mirrors both individually and of the device as a whole at an operating wavelength or close to it. The following problems are solved at this device manufacturing stage: instrument alignment to achieve the minimum focal spot size; determining focal spot size; calibration of piezoactuators to provide final mirror alignment on the synchrotron, and relevant software. For this purpose, we use a previously created X-ray optical

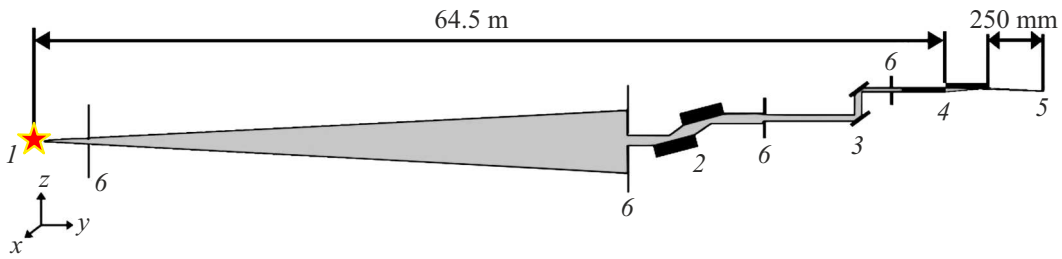

Figure 1. X-ray optical configuration of station 1-1-1: *1* — SR source, undulator; *2* — double-mirror monochromator with multilayer X-ray mirrors; *3* — slotted crystal monochromator; *4* — focusing KB system; *5* — SR focusing region; *6* — slits.

laboratory bench with a 0.154 nm (8047.8 eV) collimated X-ray beam. A collimating KB system is the „heart“ of the bench that gives a collimated $244 \times 244\,\mu$m beam with a divergence less than $\pm 10\,\mu$rad and a microfocus X-ray tube with a $8 \times 8\,\mu$m source. A collimating system used downstream of the X-ray tube made it possible to effectively „move away“ the light source by approximately 20 m with the intensity maintained at a sufficient level for precision measurements, thus bringing the laboratory experiment conditions closer to the synchrotron conditions.

This work describes the concept, construction and qualification of the KB focusing system.

1. Design concept and components

Within the concept of station 1-1-1 [8–10], X-ray optical configuration that will use the device is shown in Figure 1. Distance from the X-ray source to the center of the KB system was $L_{\mathrm{KB}} = 64.5$ m, to the focusing point from the outlet end of mirror M2 was $L_{\mathrm{PF}} = 250$ mm. Dimensions of the source at half maximum of intensity are $32.9 \times 5.9\,\mu$m in the operating photon energy range. 10−30 keV.

The following approaches were used in the focusing system design.

1. To ensure effective operation of the device in a wide photon energy range, platinum was chosen as a reflective coating material to provide the largest operating angle equal to $\vartheta = 0.15°$.

2. When choosing the mirror length, a trade-off between the maximum receipt of light from the source, for which the mirror length shall be increased, on the one hand, and provision of a submicron focal spot size and reduction of the difference between the horizontal and vertical dimensions of the focal spot, on the other hand. These objectives are met by reducing the mirror size. A trade-off mirror length was 200 mm. X-ray configuration of the focusing system is shown in Figure 1.

3. To decrease the focal spot ellipticity taking into account the big difference between the horizontal and vertical dimensions of the source, the first mirror provides focusing in the vertical plane(horizontal orientation), the second mirror provides focusing in the horizontal plane (vertical orientation). Such mirror configuration reduces the light source ellipticity by half.

4. For fine tuning of the focal spot size, mirror holders, besides 4*D* mechanical adjusters, are equipped with piezoactuators [11] that provide *in-situ* variation of the angle of light incidence on the mirrors. Angular travel range is ± 0.13 mrad with the minimum increment of 66 nrad.

5. To ensure dimensional stability of the mirrors and optical KB system as a whole, the base plate and mirror holder components are made from materials with low thermal expansion coefficient and are attached to each other and to the device housing through polished metal balls.

6. Device housing is sealed and may be filled with inert gas or dry nitrogen through dedicated valves. Vacuum-tight windows are made of the Kapton amorphous polyimide film.

7. For fine tuning of the device's optical axis to the SR source, a precision hexapod (Newport HXP200S-MECA) is installed in the housing [12]. Linear travel range is: X, Y, $Z \pm 40$, ± 45, ± 27 mm with accuracy of $0.15\,\mu$m; angular travel range is: θX, θY, θZ ± 0.157, ± 0.14, ± 0.262 rad with accuracy of $\pm 1.17\,\mu$rad. Final submicron precision alignment of the KB system axis to the source is performed by linear movement along the X and Y axes.

8. For external vibration damping, the hexapod with the device is placed on a granite base.

Photograph with removed housing and 3D model of the focusing system in the housing are shown in Figure 3.

Elliptical mirror profiles and focal spot size were calculated according to the X-ray configurations of the SR channel and focusing system as shown in Figures 1 and 2, as well as to the predefined dimensions of the source ($32.9 \times 5.9\,\mu$m). Figure 3 shows: profile calculation results with radii of curvature for each of the mirrors (Figure 3, *a*) and a focal spot (Figure 3, *b*). As shown in Figure 3, maximum mirror profile deviations from the plane are approximately 12 and 20 μm, respectively. Focal distance of ellipse is calculated using equation $c = \sqrt{a^2 - b^2}$, where a and b are ellipse semi-axes. Knowing the profiles of the fabricated mirrors, we can calculate the ellipse-semi-axes and, consequently, the focal distance for each of the mirrors that was 570 mm and 350 mm from the center of mirrors M_1 and M_2, respectively.

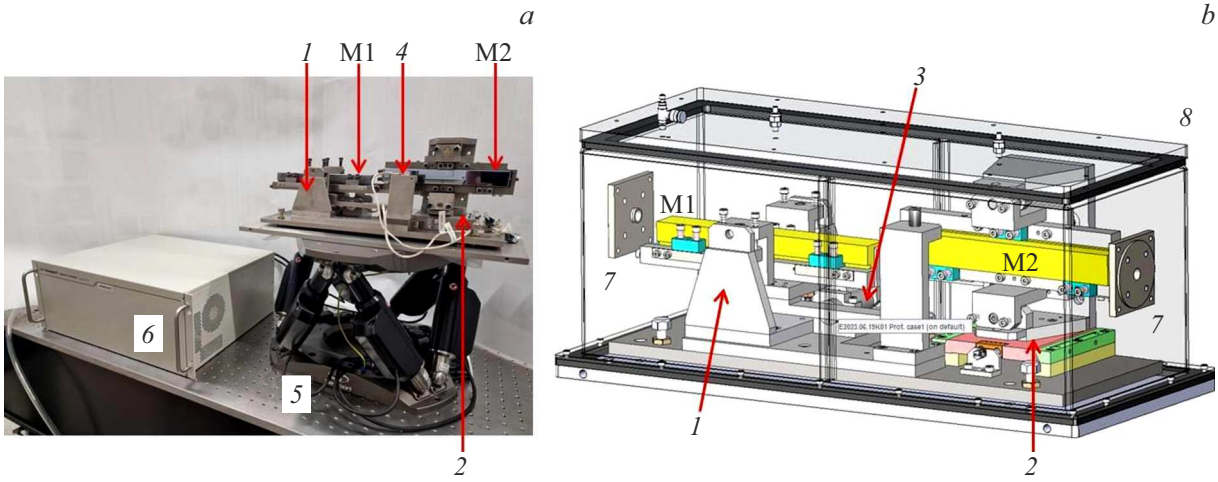

Figure 2. Photograph with removed housing (*a*) and 3*D*-model of the focusing system in the housing (*b*). M1, M2 — the first and second mirrors of the focusing KB system; *1, 2* — 4*D*mechanical adjusters of the first and second mirrors, respectively; *3, 4* — piezoactuators for fine tuning of the first and second mirror angles, respectively; *5* — Newport HXP200S-MECA hexapod; *6* — hexapod control unit; *7* — vacuum-tight windows.

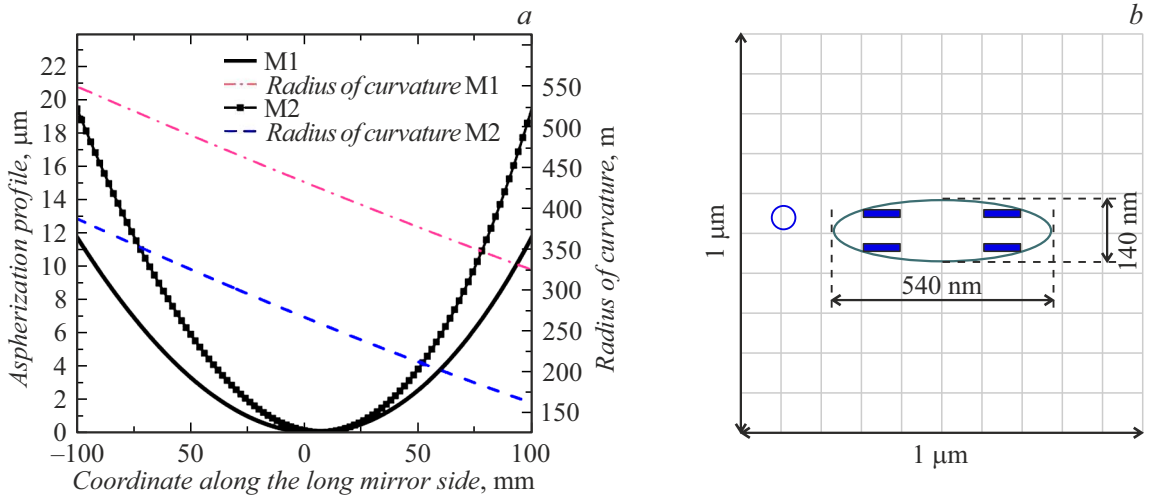

Figure 3. Aspherization profiles of mirrors M1, M2 of the focusing system with design radius of curvature for each of the mirrors (*a*) and design dimensions of the focal spot on the SR source (*b*).

Focal spot size is 140 × 540 nm. Diffraction broadening makes a significant contribution. Thus, with an energy of 10 keV, the resulting focal spot size is 250 × 580 nm instead of 140 × 540 nm, i.e.contribution to the focal point size will be made by geometrical and diffraction limitations. With 30 keV, the focused spot size is 140 × 540 nm, which is attributed exclusively to geometrical limitations.

2. Mirror fabrication

SR sources feature high radiation directivity, high mean power and high spatial radiation coherence. The employed X-ray mirrors shall meet a set of properties: withstand high absorbed radiation power, have effective roughness of 2 Åand RMS shape deviation $\leq$ 1 nm, which provides an angular error $\leq$ 1 rad. In terms of dimensional stability, single crystal silicon is the best substrate material [13–15].

For fabrication of such mirrors, a number of tasks to be solved shall be set forth: surface formation by ion-beam machining of substrates [16–18]; measurement by frame „crosslinking“ of large and aspherical mirrors with dimensions exceeding the interferometer aperture [19–22]; filtration and consideration of measurement errors related to the standard quality [22]; X-ray beam qualification of X-ray optical components [23].

Mirror substrate fabrication process may be divided into three stages: chemical-mechanical polishing [24], shaping by ion-beam machining [25] and local correction of shape errors [26].

Initial stage involves chemical-mechanical polishing (CMP) of a flat Si workpiece with a diameter of 220 mm to reduce effective surface roughness. CMP was performed on the ZPD-350 three-spindle machine designed for processing flat and spherical parts with a diameter up to 350 mm. A colloidal suspension of silicon oxide, O.P.S., was used for machining. Alupol short-flock polishing cloth was used for polishing. Polishing pad made of fabric reduces mechanical impact on the workpiece. As a results of polishing, the effective roughness is reduced from 0.37 nm to 0.21 nm in the spatial frequency range of $0.025-65\,\mu\mathrm{m}^{-1}$. Roughness was measured on the atomic force microscopy bench designed for handling large substrates [27].

Then, Si bars with desired dimensions of 200×25 mm were cut using a water jet cutting method. The next stage involved shaping using ion-beam machining with a wide-aperture source [28]. Both workpieces were preliminary measured on the Zygo Verifier plane reference wavefront interferometer with a 100 mm working aperture using the cross-linking technique [22] because the surface shape was out-of-plane and the mirror length was larger than the interferometer aperture. Measurements were also performed in several stages. Since the surface shape is out-of-plane, interference pattern may be recorded only from a small mirror area. After the measurement of a small area, the mirror was moved linearly and a new area overlapping the previous one was measured. After measuring a set of areas, the obtained data shall be preliminary processed. The images were first filtered to get rid of high frequency artefacts. The next stage considered the interferometer standard errors to obtain a more reliable result. After completion of data processing, images were crosslinked using the above-mentioned technique [22].

After measuring the surface map and 100 mm ion beam shape, a mask may be calculated. The mask is installed between the ion source and workpiece and evenly removes material from the workpiece as the latter moves linearly between the edges. To form the desired elliptical surface profile, non-uniform motion of the workpiece was used. Workpiece motion is accelerated at the edges and decelerated in the area where the major portion of material is removed. The shaping process was monitored by interferometric measurements.

Then, final machining stage is performed — correction of local shape errors using a small ion source. Before correction, the surface shape was measured using the Zygo Verifier interferometer. The measured surface error map considering the known ion beam shape (near Gaussian distribution with FWHM of 2.5 mm) was used to calculate the space-time path of the workpiece motion with respect to the ion beam, material removal was carried out along this path. During correction, the machined area of the workpiece maintains the local normal to the beam, and the material removal depth was defined by the time, when the beam was at a point.

For more details on the ion-beam etching units and local error correction, roughness measurement and surface shape, see [15,28].

This process resulted in the achievement of a surface shape with RMS deviations of 2.3 nm and 2.8 nm from the design shape for the first and second mirrors, respectively. Maps of workpiece surface shape deviation from the design shape are shown in Figure 4.

The final mirror fabrication stage involves deposition of reflective coating onto the substrate to be fabricated. For the above-mentioned spectral range 10–30 keV, platinum (Pt) is used as such coating. The Pt reflective coating was deposited by magnetron sputtering. The unit has six round planar-type magnetrons placed around a 1 m vacuum chamber (Figure 5). Targets (diameter of 150–160 mm, thicknesses up to 10 mm) are deposited onto the magnetron surface and serve as a cathode. Magnetrons are cooled by water using a pump.

The substrate is attached to a rotating disc that moves above the magnetrons. Thus, materials are deposited in a layer-by-layer manner in the case of a multilayer system. If a film is grown from only one material, one magnetron is generally used. The distance from the target to the substrate is 75 mm.

Above the working magnetrons, a glow discharge is ignited, whose ions rush towards a target with a negative potential, pick up speed and knock off atoms from the substance. The substrate is placed on the substrate holder with its working surface down. Glow discharge in the experiments with Pt had the following parameters. Discharge current — 300 mA, discharge voltage — 280 V. Film deposition rate — about 0.12 nm/h.

Shaped precision diaphragms are placed between the substrate and a magnetron located most closely to the substrate. They define the distribution of the sputtered substance flux coming onto the substrate. The shaped diaphragms are used to provide uniform distribution of the grown film with accuracy to 0.5%.

A particular diaphragm shape is determined experimentally. This is an iterative process. At the first step, the form of diaphragms is determined mathematically to provide uniformity at the level of 3%. Then, the film is sputtered on the test substrate. Mirror reflection curve is recorded by a small-angle X-ray reflectometry at different points on the substrate.

Film parameters are recovered for each point in „Multifittig“ [29]. Thus, a thickness distribution map is formed. The diaphragm shape is corrected, if required, and the deposition–measurement process is repeated until the acceptable accuracy level is achieved. After deriving the shape of diaphragms that provide coating uniformity of 0.5%, there is a thickness calibration stage. Pt film thickness was defined by the time, during which the substrate was held in the discharge zone of the corresponding magnetron. After film deposition with a discharge holding time of 15 min, a film, mirror reflection and theoretical fitting as shown in Figure 5 were obtained.

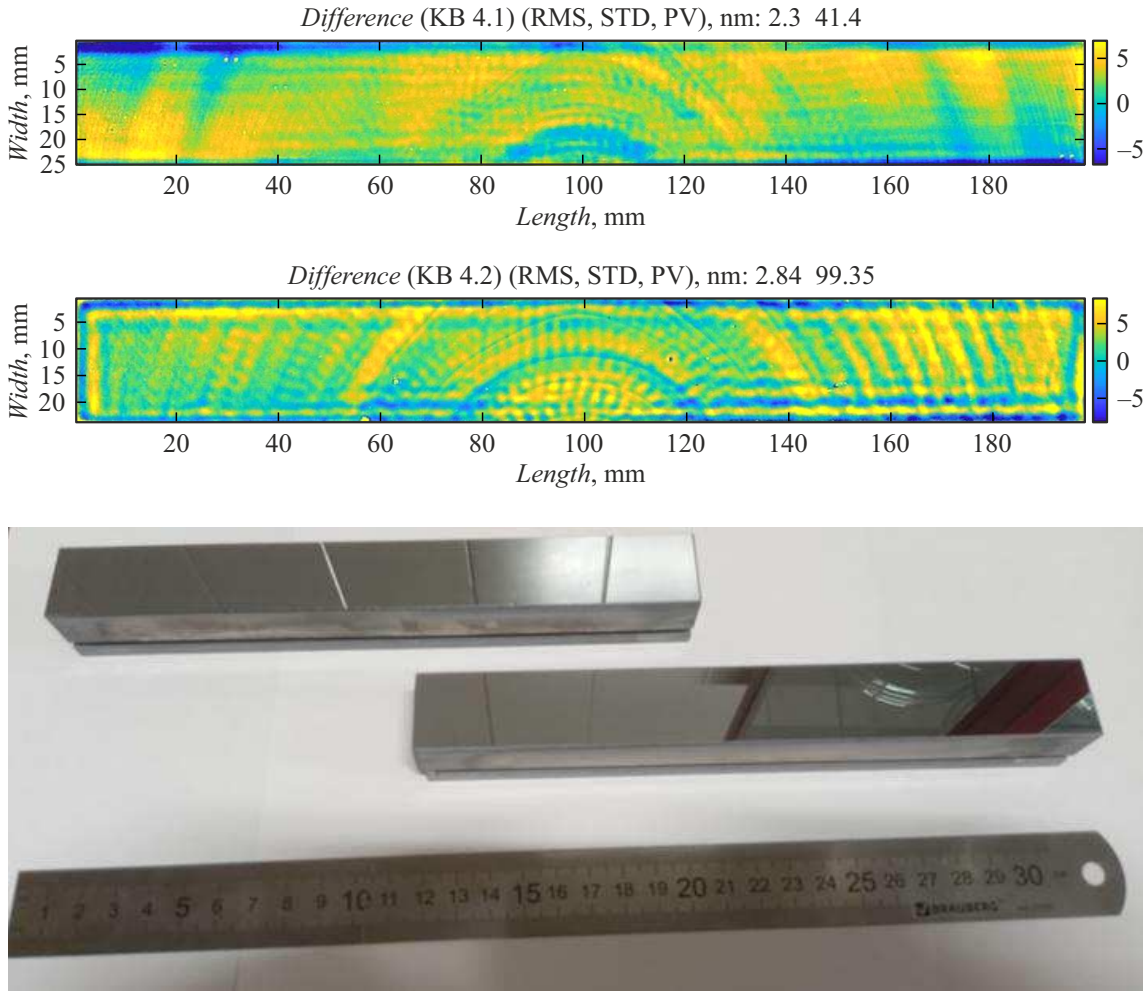

Figure 4. Maps of surface shape deviation from the design shape of mirrors M1, M2 for focusing KB system and photograph of the real mirrors.

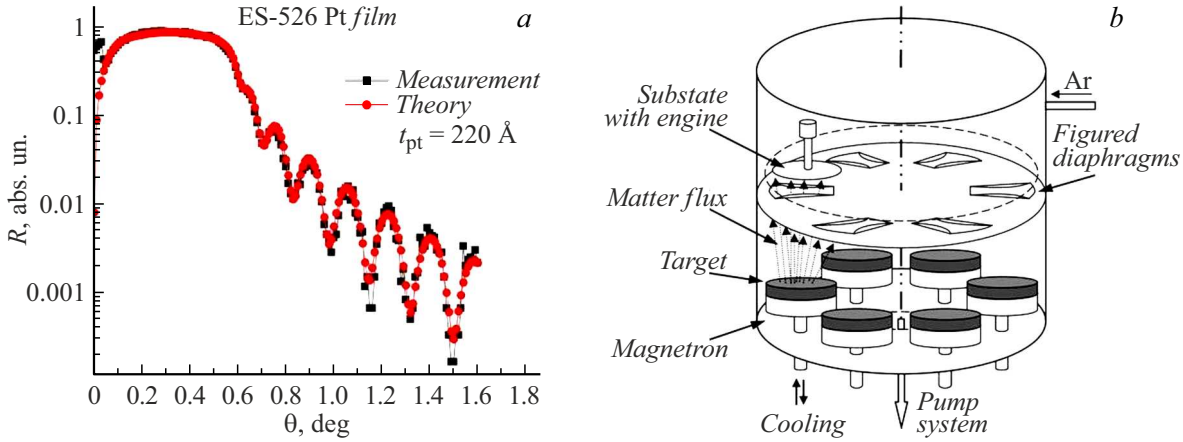

Figure 5. Mirror reflection with theoretical fitting in „Multifittig“ for 22 nm Pt film (*a*) and schematic diagram of the vacuum chamber with six magnetrons for the mirror synthesis process (*b*).

Fitting showed the film thickness of 22 nm. Therefore, 30 min is required for deposition of the desired thickness of 40 nm. It was the mode, in which Pt film was deposited on the working surface. A 10 nm Cr film was deposited beforehand to improve the adhesion between the Pt film and substrate.

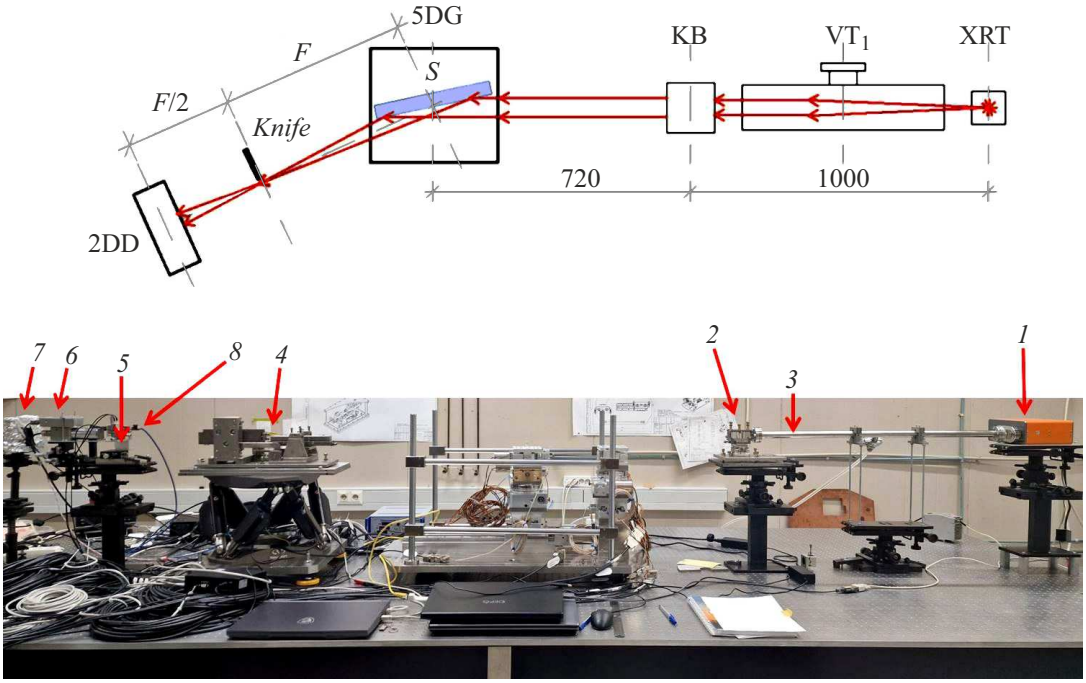

Figure 6. X-ray optical measurement bench. XRT (*1*) — the microfocus X-ray source; KB (*2*) — the collimating KB system; VT_1 (*3*) — the vacuum optical path; 5DG — the five-axis goniometer with the measured focusing KB system (*4*); Knife (*5*) — the knife with the three-axis piezoscanner; *6* — PMT; 2DD (*7*) — the two-axis matrix detector; *8* — micrometer.

3. Final qualification at the laboratory X-ray bench

X-ray beam qualification is the final stage of mirror and KB system qualification as a finished device. The problem of X-ray optics qualification at operating wavelengths is in that laboratory X-ray sources have no radiation directivity, while long (meters to tens of meters) measurement bases are required for measurements with high angular resolution. Therefore, an X-ray optical bench was preliminary designed for this purpose [23]. The main idea of this bench is in the fact that, having a microfocus X-ray radiation source, collimating optical system and vacuum tubes, a delicately diverging beam may be formed and transported at long distances. Thus, near-synchrotron conditions are provided in the laboratory. Angular divergence of such beam is defined by the source size and focal distance of the collimating system. Minimum divergence in our case was $\Delta\vartheta \approx 8\,[\mu\text{m}]/1\,[\text{m}] = 8\,\mu\text{rad}$, which in some cases is close to synchrotron beams.

The principle of operation is as follows. The collimating KB system is exposed to X-ray source (XRT) radiation (Figure 6). The MICROBOX 100 microfocus X-ray tube with a copper anode (Cu Kα characteristic line, $\lambda = 0.154\,\text{nm}$ or $8047.8\,\text{eV}$) and a source size of $8 \times 18\,\mu\text{m}$ with a tube power of 7.5 W serves as an X-ray source. Collimating system mirrors have a form of Pt-coated parabolic cylinders. Mirrors were fabricated using the above-mentioned techniques. Collimating KB system forms a $244 \times 244\,\mu\text{m}$ collimating X-ray beam both downstream of KB and at a distance longer than 3 m. The studied focusing mirror or KB (S) system as a whole is brought to the probe beam using the hexapod.

To find the focusing caustic region, a matrix detector was placed downstream of the focusing mirror at various (from 300 mm to 650 mm) distances from the mirror. The GSENSE2020BSI sensor [30] with $6.5 \times 6.5\,\mu\text{m}$ pixel and $13.3 \times 13.3\,\text{mm}$ active region serves as a matrix detector. Therefore, we were able to write the focal spot caustic (Figure 7, *a*). A knife was placed in a region with the smallest spot similar to [31]. Knife is a 0.3 mm silicon wafer with a polished end. The end was qualified for roughness and edge chipping using the ZEISS EVO 10 scanning electron microscope. No large artefacts with sizes from $1\,\mu\text{m}$ on the gauge length of 1 mm along the edge that could affect focal spot size determination were not found at the end or edge (Figure 8). Small white inclusions are easily removable dust particles. Knife was attached at the 3*D* table with a manual coarse tuning function and fine tuning function using piezoactuators. Knife scanning of the focal spot was performed using piezoactuators. Knife position was additionally monitored using an inductive micrometer with a sensitivity of $0.05\,\mu\text{m}$.

The knife overlaps the beam at $0.5\,\mu\text{m}$ intervals and detects integral beam intensity using the scintillation (thallium-doped CsI) with a photomultiplier tube. To reduce the

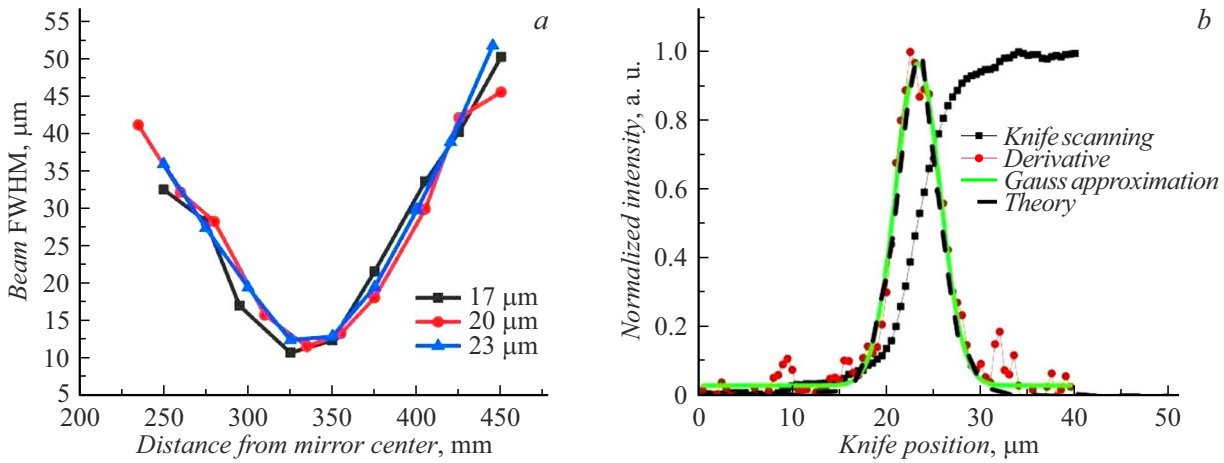

Figure 7. *a* — focal spot caustic scan by the matrix detector in different piezoactuator positions for mirror fine tuning; *b* — focal spot size measurements by the knife scanning method.

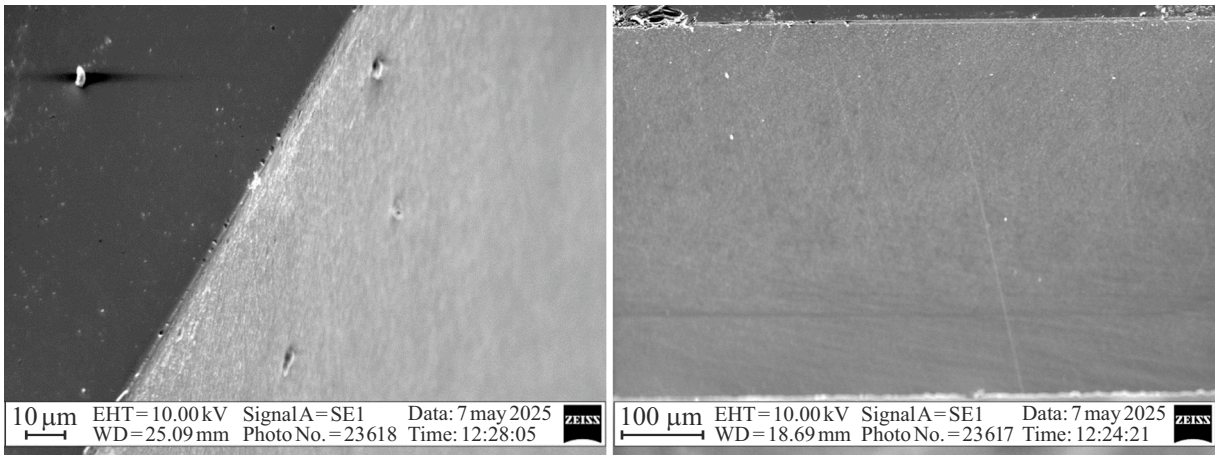

Figure 8. Knife end images recorded using the ZEISS EVO 10 scanning electron microscope. The darker region corresponds to the wafer face perpendicular to the beam.

background signal, a round diaphragm with a diameter of 1 mm was placed upstream of the detector. Consequently, an intensity drop curve is obtained from the position of the knife that gradually overlaps the beam in a direction perpendicular to the beam. This curve is differentiated and approximated by Gaussian. Thus, FWHM is the size of focal spot from the mirror (Figure 7, *b*).

A spot with a minimum size of 5.2 μm was measured. To check the obtained result, a digital twin of the measurement bench was built in SHADOWOUI ray tracing add-on [32] for OASYS [33]. Such parameters as source size, shape and divergence, mirror shape and collimating system surface shape error map were defined in the digital model. The calculation and experiment results are shown in Figure 7, *b*. The calculation result is the minimum focal spot size equal to 4.5 μm for ideal mirrors of the focusing KB system with an experimentally measured value of 5.2 μm. This focal spot broadening characterizes the mirror errors of the given focusing KB system. Within the Gaussian distribution model of the focal spot, this broadening is 2.6 μm. Thus, the focal spot size in the synchrotron channel will be approximately 2.6 μm.

Conclusion

A focusing KB system has been designed and fabricated within the work. Several measurement and engineering techniques, and an experimental equipment system have been developed during the system fabrication process. All these efforts taken together made it possible to solve the problem at a high level.

The developed ion-beam machining techniques provide an effective roughness of approximately 2 Åin the spatial frequency range of 0.025–65 μm^{-1} and shape accuracy with respect to RMSD 0.5–1 nm. Special techniques, algorithms and software were developed for measurement of substrate surfaces, including aspherical and large ones. Final qualification of the focusing properties of mirrors

was performed using an X-ray optical bench that allowed measurement of wavefront deviations with a sensitivity lower than $0.5\,\mu$rad.

Focusing properties of the KB system manufactured for the SCPS synchrotron have been studied. The focal spot size measured on the laboratory bench was $5.2\,\mu$m with a size of $4.5\,\mu$m expected for the ideal KB. The observed experimental broadening of the focal spot is explained by mirror errors of the designed KB system. Simulation in SHADOWOUI indicates that broadening observed in the laboratory corresponds to focal spot broadening on the synchrotron up to $2.6\,\mu$m. The focusing system mirror shape error maps (Figure 4) show that the main factor isn't so much the RMS error, that is equal to $2-3$ nm throughout the mirror surface and is lower than 2 nm in the working region, as the high-frequency nature of these errors. With a typical amplitude of these errors of $2-3$ nm, angular errors are equal to several microradians.

To date, the nature of these errors has been identified, corresponding corrections have been made to the fabrication process and production of a new set of mirrors has been started to provide submicrone spatial resolution.

The developed techniques and the fabrication process corrected in accordance with the investigation of the first set of focusing mirrors have become standard for manufacturing X-ray mirrors in the form of a plane, elliptical cylinders, parabolic cylinders and toroids with (sub) nanometer shape accuracy.

Funding

The study was carried out under state assignment of the Institute of Physics of Microstructures, Russian Academy of Sciences, FFUF-2024-0022, RNF 21-72-30029-P.

Acknowledgments

Focusing property testing and knife imaging results were obtained using the equipment provided by the Shared research Facility of the Institute of Physics of Microstructures, Russian Academy of Sciences.

Conflict of interest

The authors declare no conflict of interest.

References

[1] V.A. Chernov, I.A. Bataev, Ya.V. Rakshun, Yu.V. Khomyakov, M.V. Gorbachev, A.E. Trebushinin, N.I. Chkhalo, D.A. Krasnorutskiy, V.S. Naumkin, A.N. Sklyarov, N.A. Mezentsev, A.M. Korsunsky, I.P. Dolbnya. Rev. Sci. Instrum., **94**, 013305 (2023). DOI: 10.1063/5.0103481

[2] P. Kirkpatric, A.V. Baez. J. Opt. Soc. Am., **38** (9), 766 (1948). DOI: 10.1364/JOSA.38.000766

[3] V.V. Lider. Poverkhnost'. Rentgenovskie, sinhrotronnye i neitronnye issledovaniya **8**, 3 (2019) (in Russian). DOI: 10.1134/S0207352819080092

[4] E. Nazaretski, D.S. Coburn, W. Xu, J. Ma, H. Xu, R. Smith, X. Huang, Y. Yang, L. Huang, M. Idir, A. Kissa, Y.S. Chua. J. Synchrotron Radiat., **29** (5), 1284 (2022). DOI: 10.1107/S1600577522007056

[5] O. Hignette, G. Rostaing, P. Cloetens, A. Rommeveaux, W. Ludwig, A.K. Freund. Proc. SPIE, **4499**, 105 (2001). DOI: 10.1117/12.450227

[6] Ch.-Y. Huang, Ch.-Sh. Ku, Sh.-N. Hsiao, L. Lee, Sh.-J. Chiu, H.-Y. Lee, Ch.-Ch. Chen, Sh.-Ch. Chung, D.J. Wang. Energy, **1** (10), 100 (2013). DOI: 10.13140/RG.2.2.29095.55209

[7] A. Takeuchi, Y. Suzuki, H. Takano, Y. Terada. Rev. Sci. Instrum., **76** (9), 093708 (2005). DOI: 10.1063/1.2052595

[8] Ya.V. Zubavichus. *Tekhnologicheskaya infrastruktura sibirskogo kol'tsevogo istichnika fotonov „SKIF". T. 1. eksperimentalnye stantsii pervoi ocheredi i Laboratorny kompleks* (In-t kataliza im. G.K. Boreskova SO RAN, Novosibirsk, 2022) (in Russian)

[9] Ya.V. Rakshun, Yu.V. Khomyakov, E.I. Glushkov, A.S. Gogolev, M.V. Gorbachev, A.V. Dar'in, F.A. Dar'in, I.P. Dolbnya, S.V. Rashchenko, V.A. Tchernov, N.I. Chkhalo, M.R. Sharafutdinov. Izv. TPU. Inzhiniring georesursov, **336** (5), 229 (2025).(in Russian) DOI: 10.18799/24131830/2025/5/5122

[10] S.V. Rashchenko, M.A. Skamarokha, G.N. Baranov, Ya.V. Zubavichus, I.V. Rakshun. AIP Conf. Proc., **2299**, 060001 (2020). DOI: 10.1063/5.0030346

[11] Electronic source. Available at: http://www.coremorrow.com/en/proshow-11-225-1.html

[12] Electronic source. Available at: https://www.newport.com/p/HXP200S-MECA

[13] D.H. Bilderback, A.K. Freund, G.S. Knapp, D.M. Mills. J. Synchrotron Radiat., **8**, 22 (2001).

[14] H. Thiess, H. Lasser, F. Siewert. Nucl. Instrum. Meth. A., **616**, 157 (2010). DOI: 10.1016/j.nima.2009.10.077

[15] A. Erko, M. Idir, Th. Krist, A.G. Michette (editors). *Modern Developments in X-ray and Neutron Optics* (Springer, 2008)

[16] N.I. Chkhalo, I.A. Kaskov, I.V. Malyshev, M.S. Mikhaylenko, A.E. Pestov, V.N. Polkovnikov, N.N. Salashchenko, M.N. Toropov, I.G. Zabrodin. Precision Engineering, **48**, 338 (2017). DOI: 10.1016/j.precisioneng.2017.01.004

[17] M.S. Mikhailenko, A.E. Pestov, N.I. Chkhalo, M.V. Zorina, A.K. Chernyshev, N.N. Salashchenko, I.I. Kuznetsov. Appl. Opt., **61** (10), 2825 (2022). DOI: 10.1364/AO.455096

[18] N. Kumar, V.A. Volodin, S.V. Goryainov, A.K. Chernyshev, A.T. Kozakov, A.A. Scrjabin, N.I. Chkhalo, M.S. Mikhailenko, A.E. Pestov, M.V. Zorina. Nucl. Instrum. Meth. B, **534**, 97 (2023). DOI: 10.1016/j.nimb.2022.11.016

[19] F. Polack, M. Thomasset, S. Brochet, A. Rommeveaux. Nucl. Instrum. Meth. A, **616**, 207 (2010). DOI: 10.1016/j.nima.2009.10.166

[20] J. Nicolas, M.L. Ng, P. Pedreira, J. Campos, D. Cocco. Opt. Express, **26** (21), 27212 (2018). DOI: 10.1364/OE.26.027212

[21] J. Nicolas, P. Pedreira, I. Šics, C. Ramírez, J. Campos. Adv. Metrol. X-Ray and EUV Optics VI, **9962**, 996203 (2016).

[22] E.V. Petrakov, E.I. Glushkov, A.K. Chernyshev, N.I. Chkhalo. J. Surf. Invest. X-Ray Synchrotron Neutron Techn. Suppl., **18**, S58 (2024). DOI: 10.1134/S1027451024701878

[23] D.G. Reunov, A.D. Akhsakhalyan, E.I. Glushkov, I.G. Zabrodin, I.V. Malyshev, M.S. Mikhailenko, E.V. Petrakov, A.K. Chernyshev, N.I. Chkhalo. J. Surf. Invest., **18** (S1), S38 (2025). DOI: 10.1134/S1027451024701842

[24] N.I. Chkhalo, I.V. Malyshev, A.E. Pestov, V.N. Polkovnikov, N.N. Salashchenko, M.N. Toropov. UFN, **190** (1), 74 (2020).(in Russian) DOI: 10.3367/UFNr.2019.05.038601
[25] A. Chernyshev, N. Chkhalo, I. Malyshev, M. Mikhailenko, A. Pestov, N. Salashchenko, M. Toropov. Appl. Opt., **61** (33), 9879 (2022). DOI: 10.1364/AO.472504
[26] A. Chernyshev, N. Chkhalo, I. Malyshev, M. Mikhailenko, A. Pestov, R. Pleshkov, R. Smertin, M. Svechnikov, M. Toropov. Precision Eng., **69**, 29 (2021). DOI: 10.1016/j.precisioneng.2021.01.006
[27] N.I. Chkhalo, N.N. Salashchenko, M.V. Zorina. Rev. Sci. Instrum., **86**, 016102 (2015). DOI: 10.1063/1.4905336
[28] A.E. Pestov, A.K. Chernyshev, M.S. Mikhailenko, M.V. Zorina, E.I. Glushkov, E.V. Petrakov, I.V. Malyshev, N.I. Chkhalo, D.G. Reunov. Appl. Opt., **64** (4), 837 (2015). DOI: 10.1364/AO.542363
[29] M. Svechnikov. J. Appl. Cryst., **57**, 848 (2024). DOI: 10.1107/S1600576724002231
[30] Electronic source. Available at: https://www.gpixel.com/en/pro_details_1194.html
[31] H. Yumoto, H. Mimura, S. Matsuyama, H. Hara, K. Yamamura, Y. Sano, K. Ueno, K. Endo, Y. Mori, M. Yabashi, Y. Nishino, K. Tamasaku, T. Ishikawa, K. Yamauchi. Rev. Sci. Instrum., **76** (6), 063708 (2005). DOI: 10.1063/1.1922827
[32] L. Rebuffi, M. Sanchez del Rio. J. Synchrotron Rad., **23**, 1357 (2016). DOI: 10.1107/S1600577516013837
[33] L. Rebuffi, M. Sanchez del Rio. Proc. SPIE, **10388**, 103880S (2017). DOI: 10.1117/12.2274263

Translated by E.Ilinskaya